Notes on the Rabi's Cat

Das Pavel

June 19, 2024

1 Model

Parity violating Rabi model

$$\hat{H} = \omega \hat{b}^\dagger \hat{b} + \omega R \left(\hat{J}_z + j\right) + 2\sqrt{R}\lambda \left[\left(\hat{b}^\dagger + \hat{b}\right)\hat{J}_z - i\delta\left(\hat{b}^\dagger - \hat{b}^\dagger\right)\hat{J}_y\right] + \mu\left(\hat{b}^\dagger + \hat{b}\right)\left(\hat{J}_z + j\right), \tag{1}$$

- $\hat{\mathbf{J}} = \left(\hat{J}_x, \hat{J}_y, \hat{J}_z\right)$ is the quasispin (qubit) operator with size $j = 1/2$.
- $\hat{b}, \hat{b}^\dagger$ are the field (oscillator) annihilation and creation operators.
- ω is the field frequency.
- $R \gg 1$ is the detuning between the quasispin and the oscillator and plays the role of the size parameter of the system.
- λ is the quasispin-field interaction strength.
- δ interpolates between the ($\delta = 1$) Jaynes-Cummings regime, ($\delta = 0$) Rabi regime and ($\delta = -1$) anti-Jaynes-Cummings regime.
- μ governs the strength of parity-violation.

2 Critical structure

We focus on the excited-state quantum phase transition (ESQPT) at $E = 0$. Its character is given by the index k of the corresponding nondegenerate stationary point in the infinite-R limit of the Hamiltonian (1), and it changes with increasing interaction strength λ at two critical points

$$\lambda_c = \frac{\omega}{2}, \tag{2}$$

$$\lambda_0 = \frac{\lambda_c}{|\delta|}. \tag{3}$$

- $\lambda < \lambda_c$ (normal phase, N): $k = 0$, stable dynamics,
- $\lambda_c < \lambda < \lambda_0$ (superradiant phase I, S1): $k = 1$, unstable dynamics,
- $\lambda > \lambda_0$ (superradiant phase II, S2): $k = 2$, stable dynamics.

3 Local dynamics

The effective (classical) Hamiltonian is given by

$$H_{\text{eff}} = \frac{\omega}{2}\left(p^2+q^2\right) + 2\sqrt{2}j\mu q + m'\sqrt{8\lambda^2\left(q^2+\delta^2p^2\right)+\left(\frac{\omega}{2j}+2\sqrt{2}\mu q\right)^2}. \tag{4}$$

The classical dynamics is governed by the Hamiltonian equations of motion

$$\dot{\boldsymbol{x}} = \begin{pmatrix}\dot{p}\\ \dot{q}\end{pmatrix} = \begin{pmatrix}-\partial_q H_{\text{eff}}(\boldsymbol{x})\\ \partial_p H_{\text{eff}}(\boldsymbol{x})\end{pmatrix} \equiv \mathcal{F}(\boldsymbol{x}), \tag{5}$$

where $\boldsymbol{x} = (p, q)$ is the phase space vector. The local tangent dynamics is given by

$$\delta\boldsymbol{x} = \begin{pmatrix}\delta q\\ \delta p\end{pmatrix} = \mathsf{J}(\boldsymbol{x})\delta\boldsymbol{x}_0, \tag{6}$$

where

$$\mathsf{J}(\boldsymbol{x}) = \frac{\partial}{\partial\boldsymbol{x}}\mathcal{F}(\boldsymbol{x}) = \begin{pmatrix}-\partial_{pq}H_{\text{eff}} & -\partial_{qq}H_{\text{eff}}\\ \partial_{pp}H_{\text{eff}} & \partial_{pq}H_{\text{eff}}\end{pmatrix}. \tag{7}$$

The eigenvalues $\Lambda_\pm$ of the Jacobian matrix J determine the stability of the local dynamics [2, 1]: if $\Lambda_\pm$ are imaginary (conjugate), the stationary point is stable (elliptic fixed point), whereas if Λ are real, the stationary point is unstable (hyperbolic fixed point). Note that for the Hamiltonian dynamics conserving the volume of the phase space, the eigenvalues always sum to 0, so their sign must be opposite (or both are zero).

Specifically for the Rabi model (4), assuming that μ is small and can be taken as $\mu = 0$, and knowing that the stationary point we are interested in is at $q = p = 0$, the Jacobian matrix of the local dynamics is given by

$$\mathsf{J} = \begin{pmatrix}0 & -\frac{16m'j\lambda^2}{\omega}\\ \omega + \frac{16m'j\lambda^2\delta^2}{\omega} & 0\end{pmatrix} \tag{8}$$

and its eigenvalues are

$$\Lambda_\pm = \pm\frac{1}{\omega}\sqrt{-\left(16jm'\lambda^2+\omega^2\right)\left(16jm'\lambda^2\delta^2+\omega^2\right)}, \tag{9}$$

which are real for $\lambda_c < \lambda < \lambda_0$ and imaginary elsewhere. Hence for parameters (20), the local dynamics is hyperbolic with

$$\Lambda_\pm = \pm\frac{\sqrt{35}}{8} \approx \pm 0.73951; \tag{10}$$

for details see Figure 1.

The width of the initial Gaussian wave packet (coherent state) is reciprocal to the size parameter,

$$\sigma \propto \frac{1}{\sqrt{R}}, \tag{11}$$

so semiclassically for some $R > R_0$, it takes an initially narrower wave packet time Δt to reach the width of the wider wave packet for R_0,

$$\frac{\sigma}{\sigma_0} = \sqrt{\frac{R_0}{R}} = \mathrm{e}^{\Lambda\Delta t} \qquad \Longrightarrow \qquad \Delta t = \frac{1}{2\Lambda}\ln\frac{R}{R_0}. \tag{12}$$

A prominent (and easily measurable) time τ of the wave packet dynamics is when the cat dies for the first time and $q \equiv \langle\hat{\mathsf{q}}\rangle$ reaches its first minimum. It means that the wave packet leaves the

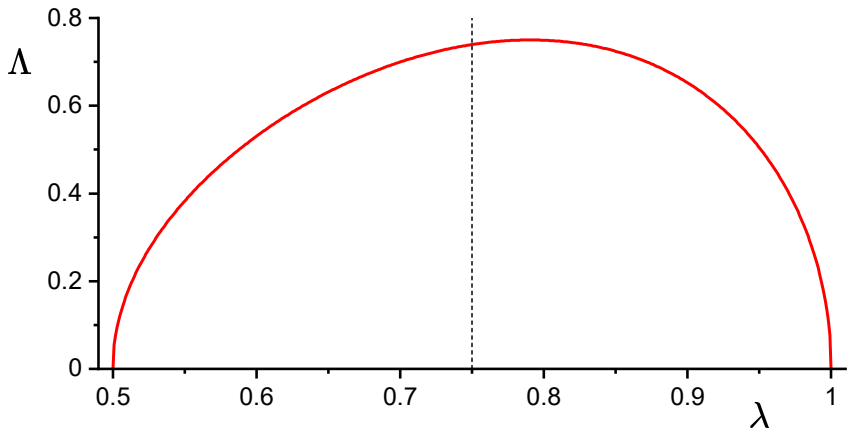

Figure 1: Dependence of the stability exponent Λ on the control parameter λ for parameters (20); the value $\lambda = 3/4$ is marked by the dashed vertical line. Maximum value $\Lambda_{\max} = \frac{3}{4}$ is reached at $\lambda_{\max} = \sqrt{5/8} \approx 0.7906$.

stationary points, makes one revolution, approaches the stationary point, and leaves it again before it localises itself in one of the wells. If this time is τ_0 for R_0, then for R it is

$$\tau = \tau_0 + 3\Delta t = \tau_0 + \frac{3}{2\Lambda} \ln \frac{R}{R_0}. \tag{13}$$

If we want the extremes of q to be at the same time for different R, we have to rescale the time, $t' = t/s$, with s given by

$$s = \frac{\tau}{\tau_0} = 1 + \frac{3}{2\Lambda\tau_0} \ln \frac{R}{R_0}. \tag{14}$$

In the rescaled time, the cat dies faster at the beginning of the second revolution if R grows because the derivative

$$\frac{\partial q(t')}{\partial t'} = \frac{\mathrm{d}t}{\mathrm{d}t'} \frac{\partial q(t)}{\partial t} = s \frac{\partial q(t)}{\partial t} \tag{15}$$

grows linearly with s. Let us denote the maximum slope (in the absolute value) of $q(t')$ as $v'_{\max}$.

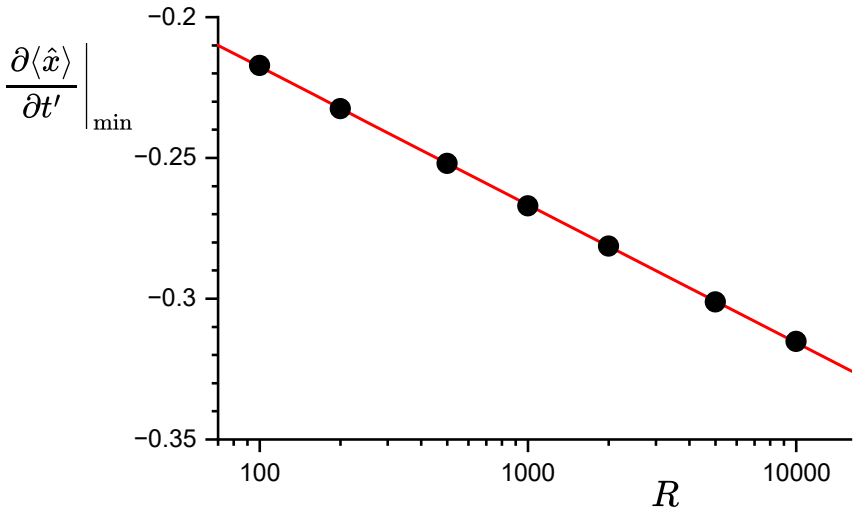

Figure 2: Dependence of the extremal slope of $q(t')$ at the time of the cat's death on the size parameter R. Numerical values for 7 different values of R are shown by black dots. The red curve depicts the fit (16) with $\alpha = -0.0490$ and $\beta = -0.120$.

Figure 2 shows how the effect of the death becomes more and more sudden. It scales logarithmically with the size parameter R,

$$\left.\frac{\partial q}{\partial t'}\right|_{\max} = v'_{\max} = \alpha \log R + \beta \tag{16}$$

(fitted values of coefficients α, β are given in the caption of the figure). On the other hand,

$$v'_{\max} = s v_{\max} = \left(1 + \frac{3}{2\Lambda\tau_0} \ln \frac{R}{R_0}\right) v_{\max}, \tag{17}$$

where we assume that $v_{\max} \equiv \left.\frac{\partial q}{\partial t'}\right|_{\max}$ is independent of R. From the last two equations, it follows that the coefficients should be

$$\alpha = \frac{3 \ln 10}{2\Lambda\tau_0} v_{\max} \approx 0.23 v_{\max} \approx -0.0499, \tag{18}$$

$$\beta = 1 - \frac{3}{2\Lambda\tau_0} \ln R_0 v_{\max} \approx 0.54 v_{\max} \approx -0.117, \tag{19}$$

that is indeed close to the fitted values. Value $v_{\max} \equiv v'_{\max}(R = 100) \approx -0.217$ was used for the numerical calculations.

4 Numerical study

In the calculations, the following values of the parameters are taken:

$$\omega = 1, \qquad \delta = \frac{1}{2}, \qquad \lambda = \frac{3}{4}, \qquad j = \frac{1}{2}, \tag{20}$$

so the system is situated in the middle of phase S1. We evolve the initially factorized state $|\psi(0)\rangle = \left|-\frac{1}{2}\right\rangle \otimes |0\rangle$ (both quasispin and field are in their lowest state) and calculate expectation values $\langle\psi(t)|\bullet|\psi(t)\rangle$ of the following operators:

- J_x (first component of the quasispin operator),
- $\hat{\mathsf{q}} = \frac{1}{2\sqrt{jR}} \left(\hat{\mathsf{b}}^\dagger + \hat{\mathsf{b}}\right)$ (coordinate related to the field).

The expectation value of both operators vanishes at all times if the parity is conserved, *i.e.*, $\mu = 0$.

5 Results

The numerical results for the expectation values of operators $\hat{\mathsf{q}}, \hat{\mathsf{J}}_x$ sensitive to the parity violation are displayed in Figures 3—6. Note that similar behaviour is observed for operators $\hat{\mathsf{p}}, \hat{\mathsf{J}}_y$. The product μR is kept constant, which makes the curves roughly coincide with one another. The value of this product is chosen so that the first significant minimum of $q(t)$ is the deepest.

Scalling $t' = t/s$ in Figures 3 and 4 is applied; the value of s is given by (14) for $R_0 = 100$ and $\tau_0 = 20.3$.

The first small dip, observed in Figure 3 (b) at $t' \approx 7$ is caused by different depths between the left and right Hamiltonian wells. This difference gets smaller with decreasing μ, and in the limit $R \to \infty$, $\mu R = \text{const}$ vanishes. On the other hand, the well-pronounced minimum at $t' \approx 20$ is caused by the phase difference between the orbits in the left and right well, and its magnitude doesn't change with μ, provided the product μR is kept constant. The same is observed for the first derivative $q'(t)$ in Figure 5.

Figure 6 shows that the first important extreme of $q(t)$ and $J_x(t)$ occurs, for a given R, approximately at the same time $t_{\min}$. There exists the smallest μ_0 for which the phenomenon is present (the centre of the leftmost lowest blue region in the second panel), and then there is a sequence of alternating minima-maxima both in q and J_x at $\mu = k\mu_0$, $k = 1, 2, 3, 4, \ldots$ .. This is related to the difference of phases between the wavepackets in both wells.

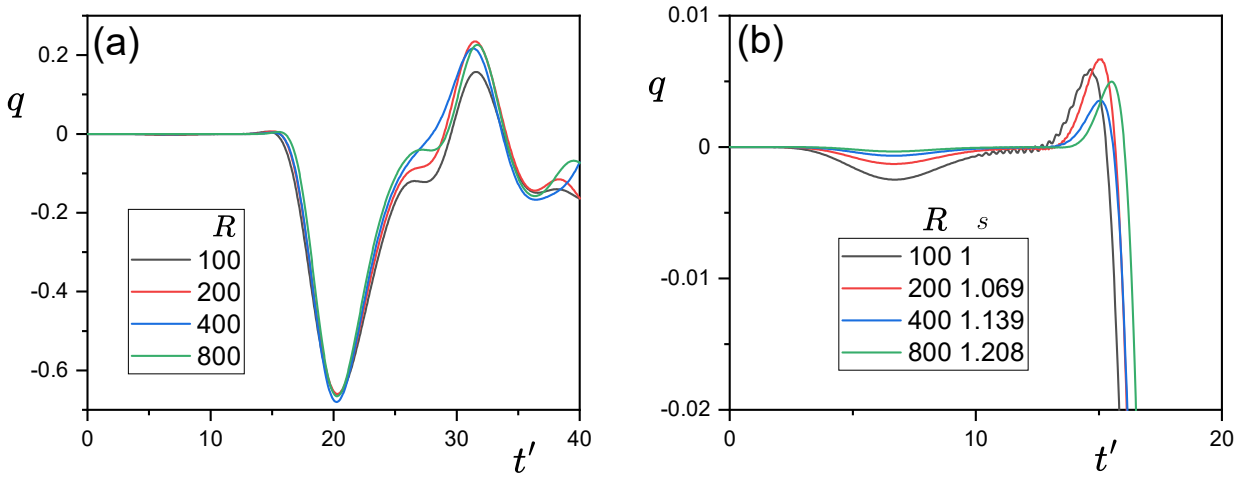

Figure 3: Expectation value $q(t) = \langle\psi(t)|\hat{\mathrm{q}}|\psi(t)\rangle$ for different system sizes R and for a perturbative value of μ reciprocal to the system size, $\mu = 0.13/R$. The magnitude of the parity violation is observed to be independent of the system size. (a) Full image. (b) Detail of the pre-parity-violation. Note that in both panels, the time is rescaled via (14) and s is indicated in the legend of panel (b).

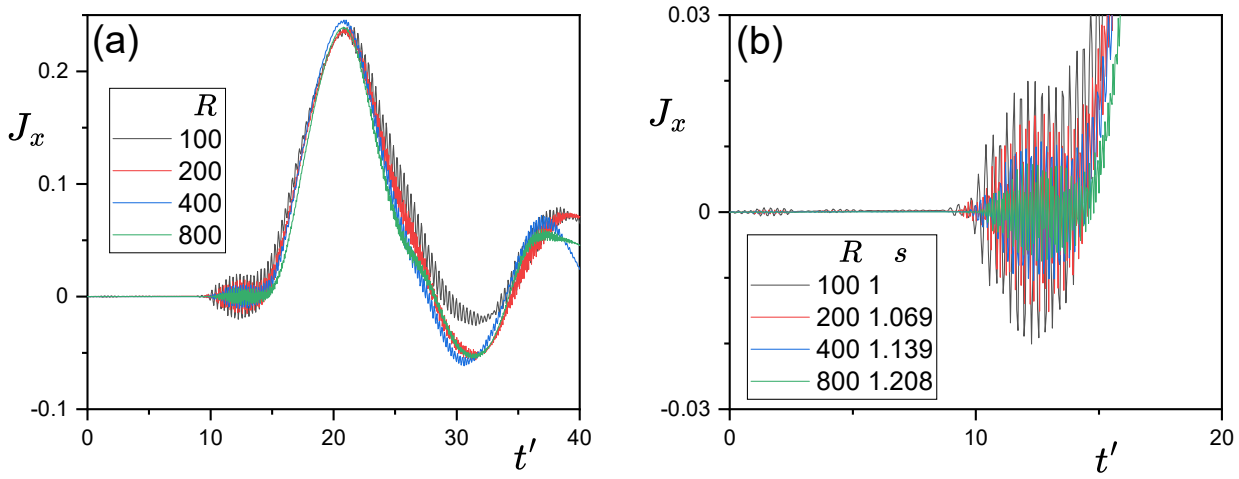

Figure 4: The same as in Figure 3, but here for expectation value $J_x(t) = \langle\psi(t)|\hat{\mathrm{J}}_x|\psi(t)\rangle$. Note the fast oscillations caused by the detuning given by parameter R.

References

[1] Saúl Pilatowsky-Cameo et al. "Positive quantum Lyapunov exponents in experimental systems with a regular classical limit". In: *Physical Review E* 101.1 (Jan. 2020), p. 010202. DOI: 10.1103/PhysRevE.101.010202.

[2] Michael Tabor. *Chaos and integrability in nonlinear dynamics. an introduction*. Wiley, 1989, p. 364. ISBN: 978-0-471-82728-3.

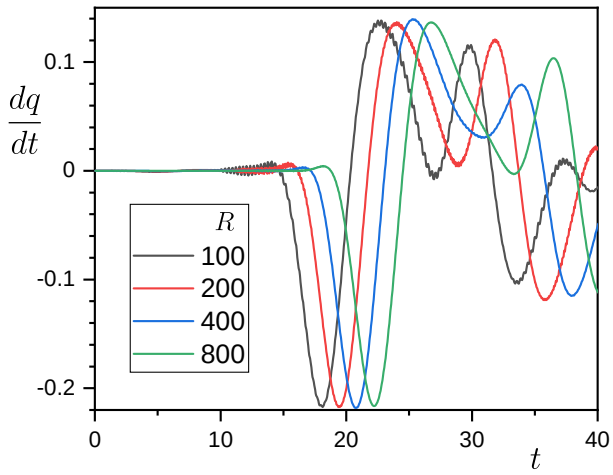

Figure 5: The first derivative of $q(t)$.

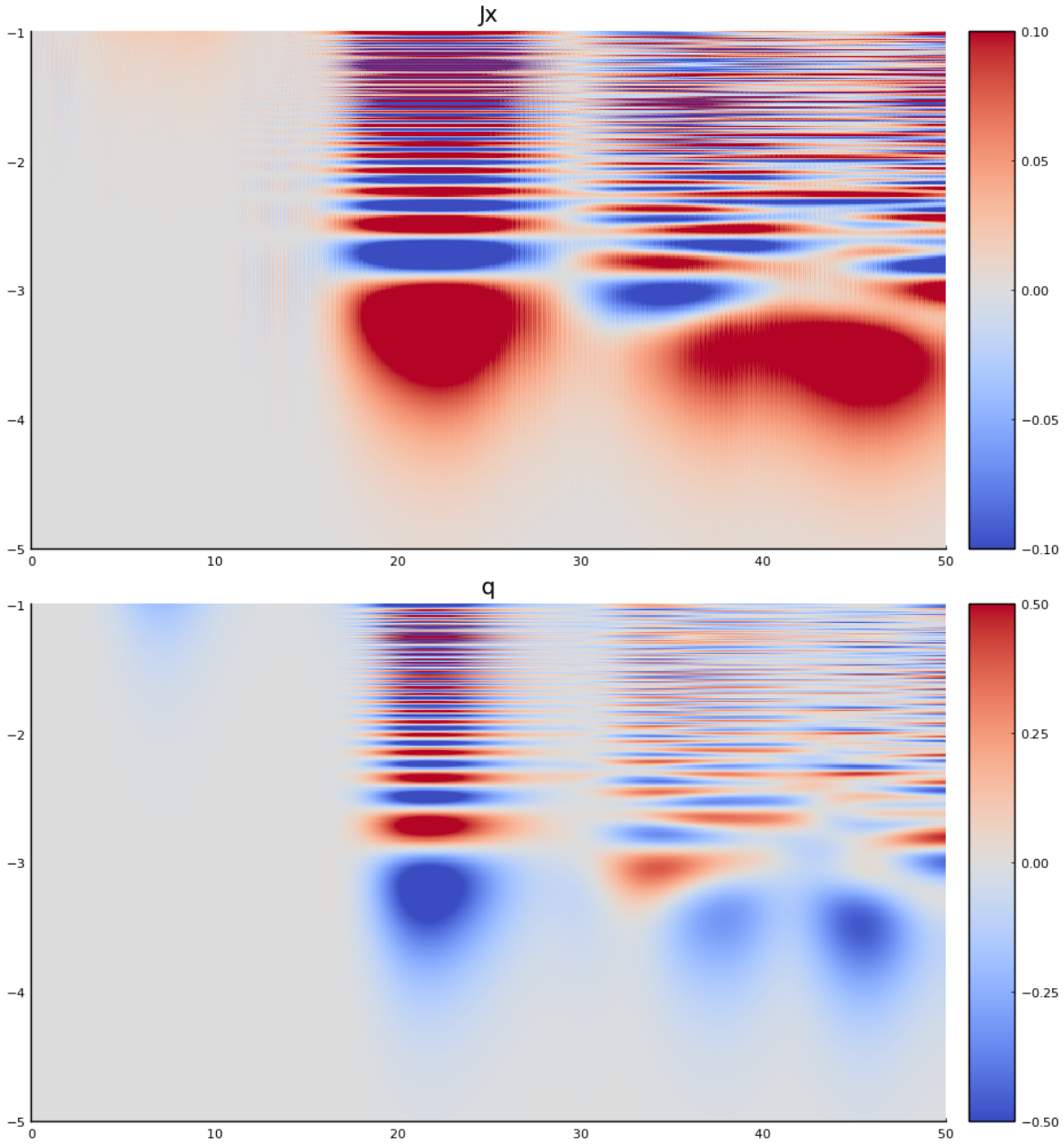

Figure 6: Full image of J_x and q as a function of t (horizontal axis) and $\log_{10}\mu$ (vertical axis) for $R = 200$.